ChemPubSoc Europe

DOI: 10.1002/chem.201704755

CHEMISTRY
A European Journal
Communication

Inorganic Complexes | *Very Important Paper*

# From a Metastable Layer to a Stable Ring: A Kinetic Study for Transformation Reactions of $Li_2Mo_3TeO_{12}$ to Polyoxometalates

Seung-Jin Oh,[a] Seong-Ji Lim,[b] Tae-Soo You,[b] and Kang Min Ok*[a]

**Abstract:** A metastable tellurite, $Li_2Mo_3TeO_{12}$, revealing a corrugated layered structure in an extremely strained coordination environment was hydrothermally synthesized in high yield. $Li_2Mo_3TeO_{12}$ undergoes $Li^+$-exchange-driven facile structural transformation reactions to polyoxometalates. The kinetic data for the transformation reactions at various conditions were successfully obtained by simple lab-source powder X-ray diffraction. The investigation suggests that the solid-state transformation reactions may occur through a series of steps; substitution, decomposition, recombination, and precipitation. This new finding could be utilized in discovering functional metastable materials as well as understanding their phase transition mechanisms.

Discovering new solid-state phases in a smart way is, an ongoing challenge for many synthetic chemists.[1] Materials with extended structures are generally prepared through standard solid-state or solvothermal reactions at high temperature and/or pressure. Therefore, the synthetic approaches often result in thermodynamically most stable crystalline compounds with global energy minima. Although a variety of kinetically stable energy states may exist,[2] the smart metastable materials have not been extensively explored attributable to the difficulty of direct observations and isolations. To monitor any possible intermediate phases and understand the mechanisms of important solid-state reactions, a number of kinetic studies for crystallizations, transformations, and intercalations, have been studied through in situ diffraction techniques thus far.[3] Most of the in situ diffraction studies, however, have been conducted using specially commissioned cells and high-energy monochromatic light sources. Herein, we report hydrothermal synthesis, structure, and characterization of a novel metastable layered tellurite and a very simple use of lab-source powder X-ray diffraction to propose a detailed transformation mechanism to thermodynamically stable polyoxometalates.

$Li_2Mo_3TeO_{12}$ was synthesized through a hydrothermal reaction by combining $Li_2MoO_4$, $MoO_3$, $TeO_2$, and $H_2O$ in a Teflon-lined autoclave at 230 °C for 1 day. Light-yellow crystals of $Li_2Mo_3TeO_{12}$ were grown in 95% yield based on $TeO_2$. Single crystal X-ray diffraction analysis indicated that $Li_2Mo_3TeO_{12}$ crystallizes in the monoclinic space group, *P*2/*c* (No. 13) and exhibited a layered structure that is composed of polyhedra with both family of second-order Jahn–Teller (SOJT)[4] distortive cations ($Mo^{6+}$ and $Te^{4+}$) and $Li^+$ cations (see Figure 1a).

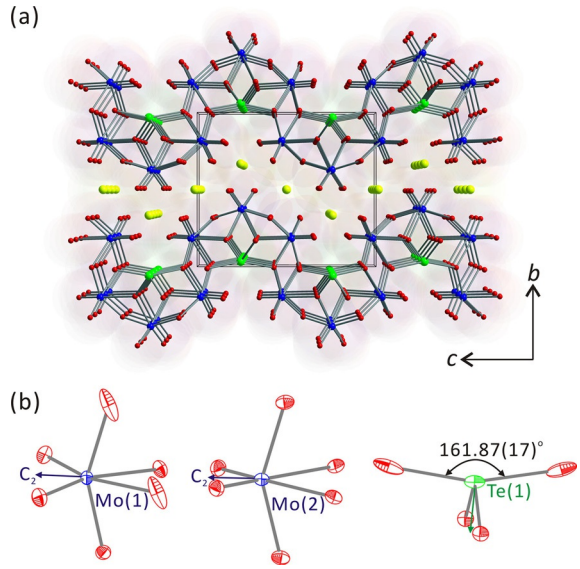


**Figure 1.** a) Ball-and-stick model of $Li_2Mo_3TeO_{12}$ revealing a corrugated layered structure in the *bc*-plane (yellow, Li; blue, Mo; green, Te; red, oxygen). b) Polyhedra with both family of SOJT distortive cations, $Mo^{6+}$ and $Te^{4+}$, exhibit highly distorted coordination environment.

Two unique $Mo^{6+}$ cations existing in an asymmetric unit are in highly distorted $MoO_6$ octahedral coordination environment with six oxide ligands. Specifically, both $Mo^{6+}$ cations are displaced toward edges of their octahedra, that is, local $C_2$-type distortions, which results in two "short" [1.709(3) and 1.731(3) Å, and 1.724(3) × 2 Å, respectively], two "intermediate" [1.932(3) and 1.954(4) Å, and 1.920(3) × 2 Å, respectively], and two "long" [2.204(4) and 2.279(3) Å, and 2.254(3) × 2 Å, respectively] Mo–O bonds. A unique $Te^{4+}$ cation is linked to four oxide ligands in $TeO_4$ seesaw moiety with two short [1.880(3) Å] and two long [2.321(4) Å] Te–O bonds. The $TeO_4$

[a] S.-J. Oh, Prof. Dr. K. M. Ok
Department of Chemistry, Chung-Ang University
Seoul 06974 (Republic of Korea)
E-mail: kmok@cau.ac.kr

[b] S.-J. Lim, Prof. Dr. T.-S. You
Department of Chemistry, Chungbuk National University
Cheongju, Chungbuk 28644 (Republic of Korea)

Supporting information and the ORCID identification number for the author of this article can be found under https://doi.org/10.1002/chem.201704755.

seesaws are in asymmetric environment as a result of the lone pair on $Te^{4+}$ cations (see Figure 1b). Two sorts of $Li^+$ cations are in $LiO_6$ coordination environment with Li-O contact distances ranging from 2.054(9) to 2.409(3) Å. The atomic Hirshfeld surface analysis on $Li_2Mo_3TeO_{12}$ also confirms all the strong and weak interactions found in the polyhedra structure. Two $Mo(1)O_6$ octahedra share their edges through O(3) and form $Mo(1)_2O_{10}$ dimers. The $Mo(1)_2O_{10}$ dimers further share their edges with $Mo(2)O_6$ octahedra through O(4) and O(5) and result in infinite chains along the *c*-axis. $TeO_4$ polyhedra then link each chain through O(3) and O(5) and form corrugated layers in the *ac*-plane. It should be noticed that the $TeO_4$ polyhedra are severely restrained. As seen in Figure 1, the $TeO_4$ seesaws are flipped over and the observed O(3)-Te(1)-O(3) angle is 161.87(17)°. The unusually distorted morphology of the $TeO_4$ polyhedra should be attributable to the smaller size of $Li^+$ cations that interact with the oxide ligands in $MoO_6$ octahedra. As seen in Figure 2, the smaller $Li^+$ cations withdraw chains of

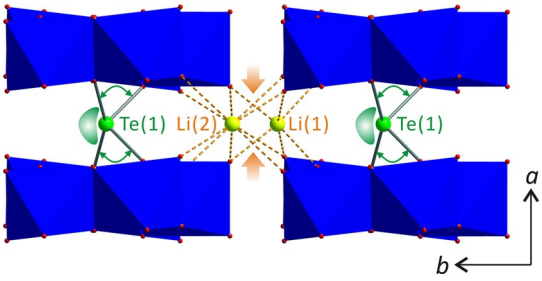


**Figure 2.** Ball-and-stick and polyhedral representation of $Li_2Mo_3TeO_{12}$ in the *ab*-plane (yellow, Li; blue, Mo; green, Te; red, oxygen). Strong interaction between smaller $Li^+$ cations and oxide ligands in chains result in a metastable layered structure containing severely distorted $TeO_4$ polyhedra.

edge-shared $MoO_6$ octahedra through substantial interactions with oxide ligands, which further causes the distortion of $TeO_4$ polyhedra. The balance between the highly strained $TeO_4$ seesaws and interactions in $LiO_6$ polyhedra certainly maintain the metastable layered structure of $Li_2Mo_3TeO_{12}$ (see Figure 2). The calculated bond valence sum value of 3.66 for $Te^{4+}$ cation and the large global instability index (GII) of 0.14, support the strained environment of $Li_2Mo_3TeO_{12}$. The lone pairs on $Te^{4+}$ cations still exist in the severely distorted $TeO_4$ polyhedra, which is confirmed by the observed Te 5*s* states at the lower energy region around −11 eV in the density of states (DOS) of $Li_2Mo_3TeO_{12}$ (see the Supporting Information). In connectivity terms, the backbone of the title material may be described as an anionic layer, $\{2[Mo(1)O_{2/1}O_{1/2}O_{3/3}]^-[Mo(2)O_{2/1}O_{2/2}O_{2/3}]^{1.333-}$-$[Te(1)O_{4/3}]^{1.333+}\}^{2-}$ and the charge balance is retained by two $Li^+$ cations located in between the layers.

The IR spectral data of $Li_2Mo_3TeO_{12}$ reveal Mo-O vibrations at ca. 851–923 $cm^{-1}$. Bands found at ca. 656–734 $cm^{-1}$ and 539 $cm^{-1}$ should be attributable to Te–O and Mo-*O*-Te vibrations, respectively.[5] The IR spectrum and its assignment are provided in the Supporting Information (Figure S2).

After taking the UV/Vis diffuse reflectance spectrum of $Li_2Mo_3TeO_{12}$, absorption data (*K*/*S*) were obtained through the Kubelka–Munk function.[6] The bandgap obtained in the (*K*/*S*) versus *R* plot for $Li_2Mo_3TeO_{12}$ was about 2.7 eV, which should be attributable to the stabilization of the relative energy arising from the interactions of the Mo–O and Te–O bonds in $MoO_6$ and $TeO_4$ polyhedra, respectively (Figure S3).

In the TGA diagram of $Li_2Mo_3TeO_{12}$, no weight loss was observed up to 730 °C. However, PXRD patterns measured at higher temperatures indicated that the title compound maintained the crystallinity up to 500 °C. Above the temperature, the material changed to an amorphous phase. The TGA data along with the variable temperature PXRD data are given in Figure S4 in the Supporting Information.

As we discussed, the title compound reveals a layered structure with highly distorted polyhedra, and the strained framework is maintained by the interactions between the small cation, $Li^+$ and oxide ligands. Thus, we thought it would be very interesting to monitor how the structural backbone will transform by exchanging the interlayer cation, $Li^+$, to other larger cations. Interestingly, all attempts to exchange the $Li^+$ for $A^+$ (A = K, Rb, and Cs) by using excess $ANO_3$ (aq.) at 90 °C for 24 h successfully produced ion-exchanged products, $A_4Mo_6Te_2O_{24}{\cdot}xH_2O$ ($x$ = 4–6). While the space groups for each product are different [$A_4Mo_6Te_2O_{24}{\cdot}6H_2O$ (A = K and Rb), $P2_1/c$;[7] $A_4Mo_6Te_2O_{24}{\cdot}4H_2O$, *Cmca*], all the ion-exchanged reaction products reveal a common structural motif, that is, polyoxometalate (POM) structure.[8]

To understand the mechanism of the transformation reactions triggered by the added alkali metal cations, we monitored the ion-exchange reactions performed at different temperatures and concentrations using lab-source PXRD. Figure 3a reveals a three-dimensional stack plot for the ion-exchange re-

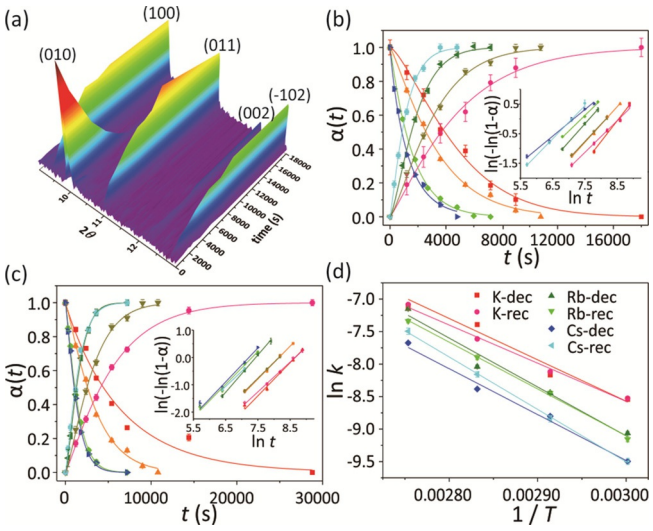


**Figure 3.** a) Three-dimensional stack plot of PXRD data obtained by analysis of materials quenched from the ion-exchange reaction of $Li_2Mo_3TeO_{12}$ with 1 M $KNO_3$ solution at 70 °C at varying time. Plot α(*t*) for the (100) and (010) Bragg reflections with respect to, b) temperature (red and pink, 60 °C; orange and dark yellow, 70 °C; green and olive, 80 °C; blue and cyan, 90 °C), and c) concentration of $KNO_3$ aqueous solution (red and pink, 0.5 M; orange and dark yellow, 1 M; blue and cyan, 2 M) at 70 °C. The insets reveal Sharp–Hancock plots for each reaction. d) Arrhenius plots to determine the activation energies for the reactions performed in 1 M $KNO_3$ solution.

action of $Li_2Mo_3TeO_{12}$ with 1 M $KNO_3$ solution at 70 °C. As seen in Figure 3a, the (010) reflection of $Li_2Mo_3TeO_{12}$ at around $2\theta = 10.0°$ decreases quickly and is not monitored after 120 min. However, other peaks corresponding to (100), (011), and (−102) reflections for $K_4Mo_6Te_2O_{24}\cdot 6H_2O$ were observed in 20th minute of the reaction at ca. $2\theta = 9.5$, 11.0, and 12.9°, respectively, and the intensity of the peaks increases over the next 180 min and then remains constant. After integrating the areas of Bragg reflections, the values were converted to extent of reaction ($\alpha$) and plotted with respect to time (see Figure 3b). In the PXRD data, no crystalline intermediates are observed and the $\alpha(t)$ curves for each phase cross near 0.5, which indicate that the conversion reaction from $Li_2Mo_3TeO_{12}$ to $K_4Mo_6Te_2O_{24}\cdot 6H_2O$ should proceed directly. Similar experiments were performed at temperature ranges from 60 to 90 °C and monitored by PXRD. As seen in Figure 3b, the reaction rates increase with increasing temperatures. To obtain mechanistic information such as the value of the reaction exponent ($n$) and the rate constant ($k$) from the experiments, the Avrami–Erofe′ev model[9] along with a Sharp–Hancock plot was utilized (inset of Figure 3b). The kinetic data for the transformation reaction from $Li_2Mo_3TeO_{12}$ to $K_4Mo_6Te_2O_{24}\cdot 6H_2O$ is summarized in Table 1. Here, the terms "decomposition" and "recombination" refer to the decay of the starting material and the growth of the product, respectively. Detailed experimental and analysis procedure in obtaining various kinetic data can be found in the Supporting Information.

**Table 1.** Kinetic parameters for the decomposition of $Li_2Mo_3TeO_{12}$ and recombination of $K_4Mo_6Te_2O_{24}\cdot 6H_2O$ as a function of temperature in 1 M $KNO_3$ solutions.

| Reactions | $T$ [°C] | $n$ | $k$ [$10^{-13}$ $s^{-1}$] | $t_{0.5}$ [s] |
|---|---|---|---|---|
| dec[a] | 60 | 1.37 ± 0.08 | 0.195 ± 0.005 | 3930 |
| rec[b] | | 1.15 ± 0.06 | 0.198 ± 0.005 | 2513 |
| dec | 70 | 1.18 ± 0.05 | 0.284 ± 0.007 | 2580 |
| rec | | 1.27 ± 0.06 | 0.298 ± 0.007 | 2513 |
| dec | 80 | 1.04 ± 0.03 | 0.617 ± 0.011 | 1138 |
| rec | | 1.32 ± 0.05 | 0.495 ± 0.010 | 1530 |
| dec | 90 | 0.93 ± 0.04 | 0.79 ± 0.02 | 849 |
| rec | | 1.16 ± 0.04 | 0.838 ± 0.019 | 870 |

[a] Decomposition. [b] Recombination.

As seen in Table 1, the Avrami reaction exponent value ($n$) varies from 0.93 to 1.37 over the studied temperature range. The result indicates that the reactions are controlled by a deceleratory process in one-dimensional diffusion because most of the observed $n$ values are $>1$. Plots of $\alpha(t)$ versus $t/t_{0.5}$ are superimposable, which confirms that the reactions occurred through the same mechanism as temperature increases (see Figure S17 in the Supporting Information). In addition, since the two curves cross near at $\alpha(t) = 0.5$ are essentially mirror images of each other for a solid-solid transformation, the fitted kinetic parameters for each pair are similar (see Table 1).

Because the decomposed fragments are assembled with introduced alkali metal cations to form POMs, similar experiments were also performed at 70 °C and monitored by PXRD to understand the effect of $KNO_3$ concentration on the rate of transformation from $Li_2Mo_3TeO_{12}$ to $K_4Mo_6Te_2O_{24}\cdot 6H_2O$. As seen in Figure 3c, the reaction rates increase as more concentrated $K^+$ ions are introduced. However, the reaction rate did not increase when the concentration of $KNO_3$ solution exceeds 2.0 M, which might be attributed to the saturation of reaction sites in $Li_2Mo_3TeO_{12}$. Plots of $\alpha(t)$ versus $t/t_{0.5}$ were also superimposable, which confirms that the same mechanism is operational (see Figure S17). A more detailed kinetic information for the transformation reaction as a function of $KNO_3$ concentration is found in the Supporting Information.

The kinetic data also indicate that the reaction rates decrease with increasing the cation size [$k(K^+) > k(Rb^+) > k(Cs^+)$]. It would be very difficult for larger cations to reach to the locations of $Li^+$ through the interlayer space. Specifically, the decomposition of $Li_2Mo_3TeO_{12}$ is strongly influenced by the substitution of $Li^+$ to other larger cations. As we mentioned previously, the corrugated layer structure of $Li_2Mo_3TeO_{12}$ in a strong structural stress due to the highly distorted $MoO_6$ and $TeO_4$ polyhedra with high GII value is maintained by interactions between the smaller cation, $Li^+$ and the framework. Once the larger alkali metal cations approach, the layered backbone decomposes to relieve the stress. The values of activation energy ($E_a$) calculated via the Arrhenius equation using the obtained kinetic data become larger with increasing the cation size, which is consistent with the substitution rates depending on the size of alkali metal cations (see Figure 3d and Table 2).

**Table 2.** Activation energies calculated by the Arrhenius equation for each ion-exchange reaction of $Li_2Mo_3TeO_{12}$ using different alkali metal cations.

| | $K^+$ | $Rb^+$ | $Cs^+$ | Reactions |
|---|---|---|---|---|
| $E_a$ [kJ $mol^{-1}$] | 53 ± 8 | 63 ± 7 | 59 ± 5 | dec[a] |
| | 49 ± 3 | 59.9 ± 1.8 | 67.1 ± 1.4 | rec[b] |

[a] Decomposition. [b] Recombination.

Considering the obtained kinetic data, a plausible mechanism for the transformation reactions from $Li_2Mo_3TeO_{12}$ to $A_4Mo_6Te_2O_{24}\cdot xH_2O$ can be suggested. The transformation reactions might occur through the following four steps, that is, substitution, decomposition, recombination, and precipitation (see Figure 4).

As described before, the reactions are presumed to be initiated by a substitution of $Li^+$ cations for other alkali metal cations, which breaks the Te–O and Mo–O bonds in the respective polyhedra [substitution ($k_{sub}$):

$$Li_2Mo_3TeO_{12} + xANO_3 \rightarrow (Li_{1-x}A_x)_2Mo_3TeO_{12} + xLiNO_3]$$

Once the bond breaking occurs, the corrugated layers decompose to $[Mo_3TeO_{12}]^{2-}$ polyhedra [decomposition ($k_{dec}$):

$$(Li_{1-x}A_x)_2Mo_3TeO_{12} \rightarrow Li_{2-2x}Mo_{3-3x}Te_{1-x}O_{12-12x} + xA^+ + x[Mo_3TeO_{12}]^{2-}]$$

Each $[Mo_3TeO_{12}]^{2-}$ polyhedron subsequently may recombine and form $[Mo_6Te_2O_{24}]^{4-}$ rings [recombination ($k_{rec}$):

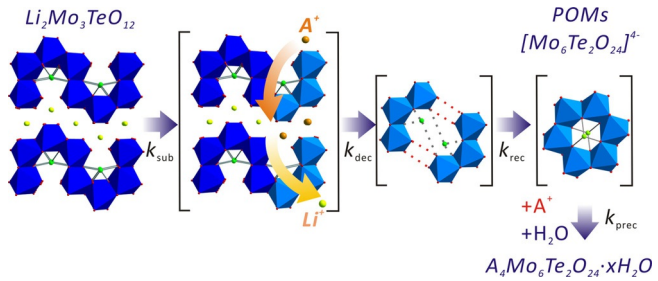


**Figure 4.** A proposed reaction mechanism for the transformation of metastable layered $Li_2Mo_3TeO_{12}$ to thermodynamically stable polyoxometalates, $A_4Mo_6Te_2O_{24}{\cdot}xH_2O$. The transformation may occur through the substitution ($k_{sub}$), decomposition ($k_{dec}$), recombination ($k_{rec}$), and precipitation ($k_{prec}$) steps.

$$2[Mo_3TeO_{12}]^{2-} \rightarrow [Mo_6Te_2O_{24}]^{4-}]$$

Finally, each $[Mo_6Te_2O_{24}]^{4-}$ ring precipitates with alkali metal cations and water revealing the POM structure [precipitation ($k_{prec}$):

$$[Mo_6Te_2O_{24}]^{4-} + 4A^+ + xH_2O \rightarrow A_4Mo_6Te_2O_{24}{\cdot}xH_2O]$$

The substitution step ($k_{sub}$) should be the rate determining step. As soon as the $Li^+$ cations are substituted, the following reactions occur promptly; thus, $k_{dec}$, $k_{rec}$, and $k_{prec}$ are much faster than $k_{sub}$.

The metastability and thermodynamic stability of $Li_2Mo_3TeO_{12}$ and the POMs, respectively, were also confirmed further. As we indicated previously, $Li_2Mo_3TeO_{12}$ was synthesized hydrothermally at 230 °C for 1 day. Once the reaction was performed for 7 days under the same reaction condition, a new tellurite, $Li_4Mo_6Te_2O_{24}{\cdot}H_2O$, with a POM structure was obtained (see the Supporting Information). In addition, if the isolated $Li_2Mo_3TeO_{12}$ was heated at 230 °C under a hydrothermal condition, $Li_4Mo_6Te_2O_{24}{\cdot}H_2O$ was synthesized as well. Therefore, it can be concluded that while $Li_2Mo_3TeO_{12}$ is a kinetic compound, $Li_4Mo_6Te_2O_{24}{\cdot}H_2O$ is a thermodynamically stable product.

In summary, we have successfully synthesized a new metastable molybdenum rich tellurite, $Li_2Mo_3TeO_{12}$ through a hydrothermal reaction. The corrugated anionic layer with severely strained polyhedra in the title compound is well maintained through interactions between smaller $Li^+$ cations and the anionic framework. $Li_2Mo_3TeO_{12}$ undergoes facile structure transformation reactions from 2D to POMs (0D) upon exchanging the $Li^+$ cations for larger alkali metal cations. Important kinetic parameters and associated thermodynamic characteristics for the solid-state reactions performed at a variety of temperatures and concentrations were successfully obtained by simple PXRD measurements. The data indicate that the structural transformation rates increase with decreasing the cation size or with increasing the concentration of added cations, which is consistent with the calculated values of the activation energy. The observations suggest that 2D $Li_2Mo_3TeO_{12}$ transforms to molecular $A_4Mo_6Te_2O_{24}{\cdot}xH_2O$ via substitution, decomposition, recombination, and precipitation steps in order. This investigation should offer not only a new soft synthetic method to design new types of POMs, but suggest a novel concept for the transformation reaction from a metastable structure to a thermodynamically stable structure.

## Acknowledgements

This research was supported by the National Research Foundation of Korea (NRF) funded by the Ministry of Science and ICT (Grant Nos. 2016R1A2A2A05005298 and 2015R1A1A1A05027845).

## Conflict of interest

The authors declare no conflict of interest.

**Keywords:** kinetics · lithium · metastable tellurites · molybdenum · X-ray diffraction

[1] a) J.-H. Feng, C.-L. Hu, X. Xu, F. Kong, J.-G. Mao, *Inorg. Chem.* **2015**, *54*, 2447 – 2454; b) H. Yu, W. Zhang, J. Young, J. M. Rondinelli, P. S. Halasyamani, *Adv. Mater.* **2015**, *27*, 7380 – 7385; c) L. Liu, Y. Yang, X. Dong, B. Zhang, Y. Wang, Z. Yang, S. Pan, *Chem. Eur. J.* **2016**, *22*, 2944 – 2954; d) Y. Wang, S. Pan, *Coord. Chem. Rev.* **2016**, *323*, 15 – 35; e) L. Li, Y. Wang, B.-H. Lei, S. Han, Z. Yang, K. R. Poeppelmeier, S. Pan, *J. Am. Chem. Soc.* **2016**, *138*, 9101 – 9104; f) M.-L. Liang, C.-L. Hu, F. Kong, J.-G. Mao, *J. Am. Chem. Soc.* **2016**, *138*, 9433 – 9436; g) M. A. Silver, S. K. Cary, J. A. Johnson, R. E. Baumbach, A. A. Arico, M. Luckey, M. Urban, J. C. Wang, M. J. Polinski, A. Chemey, G. Liu, K.-W. Chen, S. M. Van Cleve, M. L. Marsh, T. M. Eaton, L. J. van de Burgt, A. L. Gray, D. E. Hobart, K. Hanson, L. Maron, F. Gendron, J. Autschbach, M. Speldrich, P. Koegerler, P. Yang, J. Braley, T. E. Albrecht-Schmitt, *Science* **2016**, *353*, aaf3762; h) F.-F. Mao, C.-L. Hu, X. Xu, D. Yan, B.-P. Yang, J.-G. Mao, *Angew. Chem. Int. Ed.* **2017**, *56*, 2151 – 2155; *Angew. Chem.* **2017**, *129*, 2183 – 2187; i) M. R. Linaburg, E. T. McClure, J. D. Majher, P. M. Woodward, *Chem. Mater.* **2017**, *29*, 3507 – 3514; j) T. T. Tran, N. Z. Koocher, J. M. Rondinelli, P. S. Halasyamani, *Angew. Chem. Int. Ed.* **2017**, *56*, 2969 – 2973; *Angew. Chem.* **2017**, *129*, 3015 – 3019; k) J. Zhao, S. M. Islam, S. Hao, G. Tan, C. C. Stoumpos, C. Wolverton, H. Chen, Z. Luo, R. Li, M. G. Kanatzidis, *J. Am. Chem. Soc.* **2017**, *139*, 12601 – 12609; l) B. Zhang, G. Shi, Z. Yang, F. Zhang, S. Pan, *Angew. Chem. Int. Ed.* **2017**, *56*, 3916 – 3919; *Angew. Chem.* **2017**, *129*, 3974 – 3977.

[2] a) M. Jansen, I. V. Pentin, J. C. Schoen, *Angew. Chem. Int. Ed.* **2012**, *51*, 132 – 135; *Angew. Chem.* **2012**, *124*, 136 – 139; b) A. Bach, D. Fischer, M. Jansen, *Z. Anorg. Allg. Chem.* **2013**, *639*, 465 – 467; c) M. Jansen, *Adv. Mater.* **2015**, *27*, 3229 – 3242; d) Y. Wang, J. Zhu, W. Yang, T. Wen, M. Pravica, Z. Liu, M. Hou, Y. Fei, L. Kang, Z. Lin, C. Jin, Y. Zhao, *Nat. Commun.* **2016**, *7*, 12214; e) J. Ludwig, S. Gepraegs, D. Nordlund, M. M. Doeff, T. Nilges, *Inorg. Chem.* **2017**, *56*, 10950 – 10961.

[3] a) F. Millange, M. I. Medina, N. Guillou, G. Ferey, K. M. Golden, R. I. Walton, *Angew. Chem. Int. Ed.* **2010**, *49*, 763 – 766; *Angew. Chem.* **2010**, *122*, 775 – 778; b) K. M. O. Jensen, M. Christensen, P. Juhas, C. Tyrsted, E. D. Boejesen, N. Lock, S. J. L. Billinge, B. B. Iversen, *J. Am. Chem. Soc.* **2012**, *134*, 6785 – 6792; c) K. M. Ok, D. W. Lee, R. I. Smith, D. O'Hare, *J. Am. Chem. Soc.* **2012**, *134*, 17889 – 17891; d) S. J. Sedlmaier, S. J. Cassidy, R. G. Morris, M. Drakopoulos, C. Reinhard, S. J. Moorhouse, D. O'Hare, P. Manuel, D. Khalyavin, S. J. Clarke, *J. Am. Chem. Soc.* **2014**, *136*, 630 – 633; e) S. J. Moorhouse, Y. Wu, H. C. Buckley, D. O'Hare, *Chem. Commun.* **2016**, *52*, 13865 – 13868; f) Y. Wu, M. I. Breeze, G. J. Clarkson, F. Millange, D. O'Hare, R. I. Walton, *Angew. Chem. Int. Ed.* **2016**, *55*, 4992 – 4996; *Angew. Chem.* **2016**, *128*, 5076 – 5080; g) Y. Wu, S. Henke, G. Kieslich, I. Schwedler, M. Yang, D. A. X. Fraser, D. O'Hare, *Angew. Chem. Int. Ed.* **2016**, *55*, 14081 – 14084; *Angew. Chem.* **2016**, *128*, 14287 – 14290; h) H. H. M. Yeung, Y. Wu, S. Henke, A. K. Cheetham, D. O'Hare, R. I. Walton, *Angew. Chem. Int. Ed.*

**2016**, *55*, 2012 – 2016; *Angew. Chem.* **2016**, *128*, 2052 – 2056; i) D. S. Cook, Y. Wu, K. Lienau, R. More, R. J. Kashtiban, O. V. Magdysyuk, G. R. Patzke, R. I. Walton, *Chem. Mater.* **2017**, *29*, 5053 – 5057; j) J.-L. Mi, P. Noerby, M. Bremholm, B. B. Iversen, *Chem. Mater.* **2017**, *29*, 5070 – 5079; k) S. L. Skjaervø, S. Sommer, P. Norby, E. D. Bojesen, T. Grande, B. B. Iversen, M.-A. Einarsrud, *J. Am. Ceram. Soc.* **2017**, *100*, 3835 – 3842.

[4] a) U. Opik, M. H. L. Pryce, *Proc. R. Soc. London Ser. A* **1957**, *238*, 425 – 447; b) R. F. W. Bader, *Can. J. Chem.* **1962**, *40*, 1164 – 1175; c) R. G. Pearson, *J. Am. Chem. Soc.* **1969**, *91*, 4947 – 4955; d) R. G. Pearson, *J. Mol. Struct.* **1983**, 103, 25 – 34; e) R. A. Wheeler, M.-H. Whangbo, T. Hughbanks, R. Hoffmann, J. K. Burdett, T. A. Albright, *J. Am. Chem. Soc.* **1986**, *108*, 2222 – 2236.

[5] V. Balraj, K. Vidyasagar, *Inorg. Chem.* **1999**, *38*, 1394 – 1400.

[6] a) P. Kubelka, F. Munk, *Z. Tech. Phys.* **1931**, *12*, 593 – 603; b) J. Tauc, *Mater. Res. Bull.* **1970**, *5*, 721 – 729.

[7] V. Balraj, K. Vidyasagar, *Inorg. Chem.* **1998**, *37*, 4764 – 4774.

[8] a) M. Ammam, *J. Mater. Chem. A* **2013**, *1*, 6291 – 6312; b) S.-S. Wang, G.-Y. Yang, *Chem. Rev.* **2015**, *115*, 4893 – 4962; c) A. Blazevic, A. Rompel, *Coord. Chem. Rev.* **2016**, *307*, 42 – 64.

[9] a) M. Avrami, *J. Chem. Phys.* **1939**, *7*, 1103 – 1112; b) M. Avrami, *J. Chem. Phys.* **1940**, *8*, 212 – 224; c) B. V. Erofe'ev, *C. R. Dokl. Acad. Sci. URSS* **1946**, *52*, 512 – 514.

Manuscript received: October 9, 2017
Accepted manuscript online: December 7, 2017
Version of record online: December 27, 2017